Colour-differential interferometry for the observation of extrasolar planets

M. Vannier, R. G. Petrov, B. Lopez, F. Millour

Mon. Not. R. Astron. Soc. **367,** 825–837 (2006) doi:10.1111/j.1365-2966.2006.10015.x

Colour-differential interferometry for the observation of extrasolar planets

M. Vannier,[1⋆] R. G. Petrov,[2] B. Lopez[3] and F. Millour[2,4]

[1]*European Southern Observatory, Casilla 19001, Santiago 19, Chile*
[2]*LUAN, Université de Nice-Sophia Antipolis, Parc Valrose, F-06108 Nice Cedex 2, France*
[3]*Observatoire de la Côte d'Azur, Département Gemini, BP 4229, F-06034, Nice Cedex 4, France*
[4]*LAOG, 414 rue de la piscine, 38100 Saint-Martin d'Hères, France*

Accepted 2005 December 15. Received 2005 December 11; in original form 2005 April 29

ABSTRACT

We present the high angular resolution technique of colour-differential interferometry for direct detection of extrasolar giant planets (EGPs). The measurement of differential phase with long-baseline ground-based interferometers in the near-infrared could allow the observation of several hot giant extrasolar planets in tight orbit around the nearby stars, and thus yield their low- or mid-resolution spectroscopy, complete orbital data set and mass. Estimates of potentially achievable signal-to-noise ratios are presented for a number of planets already discovered by indirect methods. The limits from the instrumental and atmospheric instability are discussed, and a subsequent observational strategy is proposed.

Key words: techniques: high angular resolution – techniques: interferometric – techniques: spectroscopic – planetary systems.

1 INTRODUCTION

Since the discovery of a planet around 51 Pegasi by Mayor & Queloz (1995), the indirect method of radial velocities (RV) has provided a large harvest of extrasolar planets (ESPs) detection, thus yielding orbital distance and eccentricity, and lower mass estimates. Very high accuracy astrometry is another technique to measure the reflex motion of the parent star resulting from the planet orbital motion, and should yield, unambiguously, the orbit and mass of giant planets. However, these are indirect techniques which do not give access to the ESP spectrum. For a small number of planets whose orbital plane is oriented edge-on to the Earth, a transit has been observed. For one of them (HD209458), this yielded some spectral atmospheric features in addition to the mass and radius (Brown et al. 2000), and the observation of the secondary transit gave the first estimates of the thermal emission from hot ESPs (Charbonneau et al. 2005; Deming et al. 2005).

Direct observations are in general very difficult for current instruments because of the very small angular separation between the star and the planet, and their extremely high luminosity ratio. Limiting the stellar light scattering to the telescope diffraction pattern, by observing from space or with efficient adaptive optics, could allow the detection of planets which are well angularly resolved from their star. This might be the case for a candidate planet separated by ≈780 mas (i.e. ≈55 au) from a brown dwarf, whose image and spectrum were recently obtained in the infrared (IR) with the Very Large Telescope (VLT) instrument NACO (Chauvin et al. 2004). For targets with closer angular separation and less favourable luminosity ratio, detecting planetary photons out of the noise requires to decrease the effect of the stellar light within the Airy rings. Several methods have been proposed in the last two decades for this purpose, most of them using coronography/nulling techniques with single or multiple apertures. In any case, the measurement is very challenging due to, on one hand, the limited number of photons available from the ESP and, on the other hand, the need for an accurate calibration of the instrumental stability.

In this paper, we discuss the potential of colour-differential interferometry (CDI) to directly detect the photons emitted by ESPs. CDI is based on *simultaneous* interferometric observations in different spectral channels. As a high angular resolution and high-dynamic technique, it presents two major advantages. First, the chromatic differences in visibility and phases are much less sensitive to instrumental and atmospheric instabilities, and therefore are easier to calibrate than the absolute complex visibility. Since the beginning of long-baseline optical interferometry with separated apertures, many early astrophysical results have been obtained using this self-calibration feature (e.g. Thom, Granes & Vakili 1986; Mourard et al. 1989). Secondly, the colour-differential phase can be measured with an accuracy much better than the angular interferometric resolution λ/B. For objects much smaller than the diffraction limit, it is proportional to the variation of the object photocentre with wavelength. This feature was first presented by Beckers & Hege (1982) for differential speckle interferometry and has later been developed by Petrov, Roddier & Aime (1986), Petrov (1989) and the GI2T team.

⋆E-mail: mvannier@eso.org

Therefore, differential phase is a close parent of the colour-differential astrometry method (also called sometimes spectroastrometry), based on the displacement with wavelength of the photocentre of a long exposure image at a telescope focus (Sorokin & Tokovinin 1985; Lund & Aime 1988; Takami, Bailey & Chrysostomou 2003). For diffraction-limited images, the performance of these two techniques is proportional to the square root of the number of collected photons [i.e. to the telescope diameter(s)], and to the baseline length (Petrov 1989). Thus, long-baseline interferometers have a very clear advantage compared to the equivalent single-telescope technique. The measurement of photocentre displacement can yield decisive angular information on otherwise unresolved objects. It applies to almost all types of sources where spectral features are linked to asymmetric high spatial resolution structures, including broad-line region (BLR) of active galactic nuclei (AGNs), stellar surface and activity, circumstellar material in young and evolved stars, and close binary stars with high colour difference.

Lopez & Petrov (2000) and Swain et al. (2000) have proposed to apply CDI (also called colour-differential phase technique) to objects with extremely high flux dynamics such as ESPs. They estimate that this method has some potential for observing 'Pegasi' planets, i.e. hot extrasolar giant planets (EGPs) in tight orbit, therefore strongly irradiated by their star. We investigate, hereafter, in further details the possibilities for observation of EGP using CDI.

In Section 2, we present the scientific benefits of direct observation of ESPs with the proposed method and emphasize on hot giant planets. In Section 3, the principle, formalism and fundamental noises of CDI are presented. In Section 4, we explicit the signal provided by phase and closure phase. Assuming that stability at the level of the fundamental noises can be achieved, we demonstrate how the spectrum, mass and inclination are derived from the measurements in the simple case of a circular orbit. In Section 5, we assume the use of the Very Large Telescope Interferometer (VLTI) to calculate the potential signal-to-noise ratios of the planetary spectrum for a number of known objects. The best targets for future observations are identified. The effects of astrophysical biases (including stellar rotation, stellar spots and exozodiacal light), which might affect the measurement of the planetary signal, are discussed. The issue of instrumental and atmospheric effects is presented, and an observational strategy for reaching the highest precision is proposed.

2 SCIENTIFIC CASE: DIRECT MEASUREMENT OF EGPS

To date, the RV measurements led to the discovery of 170 ESPs. RV detection yields the semimajor axis, the eccentricity and a lower value $M \sin i$ of the mass of the planet. It is estimated that at least 20 per cent of Sun-like stars have a massive planetary companion (Lineweaver & Grether 2003). RV surveys to be done with increased accuracy and over longer time-span should yield a vast sample of extrasolar planetary objects in the next years, and extend our present knowledge to planets of lower mass and/or at larger orbital radius (Cumming 2004). A large proportion of the already detected EGPs were found at a surprisingly small orbital distance a with regard to their high mass: about 30 per cent of the planets have a semimajor axis lower than 0.2 au and a mass over 0.4 $M_{\rm Jup}$ (Jupiter mass). Even though this odd statistical distribution should be handled carefully because the instrumental bias of velocimetric methods favours tight orbit and massive planets, their mere presence appeared in contradiction with the hitherto standard models of planetary formation based on the Solar System. This has raised important questions regarding the origin and formation scenario of planets, some possible migration process and their physical structures. Whereas an abundant theoretical literature on the formation and evolution of EGPs has been produced, key points are still hypothetical and would benefit from the constraints derived from direct observation: atmospheric spectra, complete orbital data, planetary mass and radius, ...

A low spectral resolution (of about a few tens) over a large bandwidth gives the general shape of the planetary spectrum. This primarily yields the effective temperature of the planet. It may also be sufficient to constrain the presence of dusty clouds in the atmosphere: current models of EGP spectrum are strongly dependent(e.g. Barman, Hauschildt & Allard 2001) on whether grain particles remain present in the atmosphere and thus contribute to its opacity ('dusty' assumption), or are removed from it by gravitational settling ('condensed'). Since this affects the radiative/convective energetic balance of the planet, evolution models indicate that the cooling and contraction time-scales may differ by factors of 2 to 3, depending on the presence of dusty clouds (Guillot 1999).

The atmospheric chemical composition can be partially inferred from spectral absorption features: in the near-IR domain and around 10 μm, molecules of H_2O, CO, CH_4 and NH_3 present numerous absorption bands and molecular lines, whose intensity depends on the relative abundance of these molecules, on their depth within the atmosphere and on the presence of higher clouds. Separating individual lines would require a spectral resolution $R > 1000$ and seems out of range for the method we propose hereafter. According to our computations, though, a few planetary candidates could be observed at a resolution $R = 1500$, which could be sufficient to partially resolve these spectral features.

Some information on the process of energy circulation within the atmosphere can be inferred from direct detection at various orbital positions in the case of EGPs with semimajor axis smaller than ≈0.07 au, which are in synchronous rotation around their star. For these objects, the mechanism of energy transfer between the bright ('day') and dark ('night') areas of the atmosphere was studied theoretically by Showman & Guillot (2002). A significant difference of temperature between the two sides is expected; thus their relative contribution to the thermal emission from the planet depends on the orbital phase and on wavelength. Although small, this effect could be constrained by comparing colour-differential measurements at several orbital positions.

Direct observation will also yield the inclination i and orientation of the planetary orbit with respect to the observer. The orientation angle of the orbit can be compared to the position angle of the stellar axis, inferred independently using CDI, as shown by Chelli & Petrov (1995b). The co-planarity between the stellar and the planetary planes might constitute a test on the origin of EGPs by distinguishing between (1) a model where the planets form in the outskirts of the protostellar disc (in a similar way as the giant planets of our Solar System) and later undergo a migration process and (2) an alternative model where giant planet arises from unstable fragmentation of the protostellar nebula, in which self-gravitating clumps may rapidly grow to large bodies in non-coplanar orbits (Mayer et al. 2002). For planets detected by RV measurements, the knowledge of the orbital inclination i would suppress the ambiguity on the planetary mass M. Theoretical models on formation and migration scenarii could therefore be tested with a more precise statistical distribution of the masses (Stepinski & Black 2000).

3 FORMALISM OF CDI FOR ESPS

3.1 Colour-differential phase and visibility

Both the European Southern Observatory (ESO) VLTI and the Keck Interferometer are now offering the possibility to observe in colour-differential interferometric mode. We hereafter assume, for the instrumental characteristics, the use of the VLTI AMBER or MIDI instruments, both of which are already available to the community of observers, in a limited number of modes. AMBER performs multi-axial combination of two or three beams in the bands J, H and K, and will yield dispersed fringes with a spectral resolution ranging from 35 to 12 000 (Petrov et al. 2003). The MIDI instrument (Leinert et al. 2003) combines two beams with a temporal fringe scanning and operates in the mid-IR N band (8–13 μm) with a spectral resolution up to 250.

Let T be the global instrumental transfer function of the whole interferometer (including the atmosphere, telescopes, interferometric delay lines and various instrumental parts down to the detector). For a source object of spatial distribution $\tilde{I}_0$ in the plane of spatial frequencies $\boldsymbol{w}$ and at wavelength λ, the image through the instrument is

$$\tilde{I}(\boldsymbol{w}, \lambda) = \tilde{I}_0(\boldsymbol{w}, \lambda)\tilde{T}(\boldsymbol{w}, \lambda). \tag{1}$$

The interferometric visibility V is defined as the normalized amplitude of $\tilde{I}(\boldsymbol{w}, \lambda)$ and the interferometric phase Φ as the argument of $\tilde{I}(\boldsymbol{w}, \lambda)$. Note with the '*' contribution from the astrophysical signal and with 't' the one from the atmospheric, telescope and instrumental transfer function. Then, the visibility and phase at that spatial frequency are

$$V = \frac{|\, I(\boldsymbol{w}, \lambda)\,|}{|\, I(\boldsymbol{0}, \lambda)\,|} = V_* V_{\rm t} \tag{2}$$

and

$$\Phi = \arg[I_0(\boldsymbol{w}, \lambda)] + \arg[T(\boldsymbol{w}, \lambda)] = \Phi_* + \Phi_{\rm t}. \tag{3}$$

In practice, the term $\Phi_{\rm t}$ is largely unknown and variable, thus the interferometric phase cannot be determined as an absolute quantity. Instead, a possibility is to measure the phase relatively between two sources using a dual-feed interferometer, such as the PRIMA device will provide to the VLTI (Derie et al. 2003). CDI presents another possibility: from a spectrally dispersed interferogram, both the visibility and the phase can be measured relatively and simultaneously between various spectral channels (say, a 'target' channel noted λ_i and a reference channel $\lambda_{\rm r}$), hence yielding the difference of interferometric phases and the ratio of visibilities between the corresponding wavelengths

$$\Delta\Phi(\lambda_i, \lambda_{\rm r}) = \left[\Phi_*(\lambda_i) - \Phi_*(\lambda_{\rm r})\right] - \left[\Phi_{\rm t}(\lambda_i) - \Phi_{\rm t}(\lambda_{\rm r})\right] \tag{4}$$

$$V(\lambda_i, \lambda_{\rm r}) = \frac{V_*(\lambda_i)}{V_*(\lambda_{\rm r})}\,\frac{V_{\rm t}(\lambda_i)}{V_{\rm t}(\lambda_{\rm r})}. \tag{5}$$

As it appears from the terms on the right-hand side of the above expressions, the observables of CDI are not affected by the *achromatic* effects from atmospheric or instrumental origin. This non-sensitivity to an otherwise dominant effects[1] is one of the great advantages of that technique, and allows to measure even small changes of phase and/or of visibility if the brightness distribution varies with wavelength.

It is common (e.g. at the VLTI and Keck Interferometer instruments) to use a spatial filtering prior to the recombination in order to clean the beam's wavefront from the atmospheric or instrumental effects. The only remaining optical effects after the spatial filter are differences in intensity between the beams (which can subsequently be calibrated thanks to photometric channels), and an OPD. In principle, this OPD originates exclusively before the filtering, from the piston and from the chromatic dispersion along the path. Therefore, it is partly chromatic and will affect the differential measurement (see Section 5.4 for quantitative detail on that aspect). In practice, imperfect adaptive optics induce wavefront corrugations which are turned into additional (chromatic) OPD by the spatial filter (as presented in detail by Tubbs et al. 2005). In the case of the VLTI with MACAO correction, that effect is marginal.[2]

In a given spectral channel, the OPD induces a phase shift of

$$\psi_{\rm OPD}(\lambda) = (2\pi/\lambda)\,{\rm OPD}. \tag{6}$$

The sensitivity of the visibility to the OPD depends on the coherence length $L = \delta\,\lambda/\lambda^2$ for a given bandwidth. The visibility varies as

$$V_{\rm OPD}(\lambda) \propto \frac{\sin(\pi\,{\rm OPD}\,\delta\lambda/\lambda^2)}{\pi\,{\rm OPD}\,\delta\lambda/\lambda^2}. \tag{7}$$

3.2 Differential visibility and phase for reaching very high precisions

In principle, the visibility and the phase carry complementary astrophysical information, and both are useful for our goal of observing ESPs. In the next section, we show that the amplitude of the signal from the visibility and the phase (without considering the atmospheric and instrumental effects) is of similar order. Nevertheless, one should wonder which of these observables is most appropriate for reaching the very high required precision of measurement. If the measurement is made in a colour-differential mode and with a spatial filtering, the precision on both the visibility and the phase is affected by the following.

(i) The fundamental noises such as photon, readout and background noises (detailed in Section 3.4). These noises affect the differential visibility and phase similarly.

(ii) The chromatic OPD between the beams, introduced by the longitudinal dispersion in the air and water vapour and by the instrument. We show that these variable chromatic effects will be significantly higher than the astrophysical signal from the differential phase, and therefore will require proper calibration and/or correction. They might be substracted from the phase measurement by using closure phase (Section 3.3), or monitored, calibrated and corrected by a post-observational fit processing on single-baseline

[1] The piston at the VLTI for a 100-m baseline is of the order of 10 μm (rms). The FINITO fringe tracker should allow one to equalize this optical path difference (OPD) down to 0.05 μm, i.e. a phase shift of ≈0.15 rad in K band. On the other hand, the effect of λ-dependent piston (i.e. the chromatic piston), measured at a worst site (Swain et al. 2000), was a few 10^{-2} rad on the differential phase in K band, i.e. 0.01 μm. See Section 5.4 for further details on the chromatic OPD.

[2] From the simulations made by Tubbs et al. (2006) and for the correction parameters at VLTI/MACAO ($D/r_0 \approx 10$ and at least 30 zernike modes suppressed by adaptive optics), the rms phase jitter is less than 0.1 rad. This is lower than the equivalent fundamental (photon) noise of our targets for an individual exposure (about 0.2 rad per spectral channel for a 25-ms frame). Therefore, this effect is marginal in the error budget.

differential phase (Section 5.4). By deriving equations (6) and (7), we find that the visibility is less sensitive (by several magnitudes) to variable chromatic OPD than the phase, whatever the considered spectral range be. Therefore, the visibility is much favoured in this respect.

(iii) Some post-filtering effects occur during the beam recombination or on the detector plane. Internal spatial modulation should allow us to correct this effect on the differential phase (see Section 5.4 for more details), but not on the differential visibility.

As a summary, the colour-differential phase and visibility will be affected differently by atmospheric and/or instrumental effects. At this stage, it is too early to estimate which of these two observables will best allow to reach the very high precision goal (see Section 5.5 for the current precisions on the AMBER instrument). In what follows, we will consider both of them, with some emphasis on the phase which, historically, has been more regarded for observing ESPs.

3.3 Closure phase

Closure phase has first been proposed for observing ESPs by Ségransan et al. (2000). If more than one interferometric baseline is available, it probably constitutes the most efficient approach for suppressing the instrumental effects on the interferometric phase.

We note as (i, j) the baseline ranging between telescopes i and j. Assuming the beams are spatially filtered, we can expand $\Phi_{t(i,j)}$ in equation (3) as

$$\Phi_{(i,j)} = \Phi_{*(i,j)} + [\psi_{\mathrm{OPD}(i,j)} + \phi_{t(i,j)}], \tag{8}$$

where $\psi_{\mathrm{OPD}(i,j)}$ is the phase term introduced by the OPD previous to the recombination of the beams (see equation 6), and $\phi_{t(i,j)}$ corresponds to the effects which occur during and after the recombination. Closure phase entirely suppresses the OPD effects by summing the pairs of baselines over a closed loop, so that the phase shifts between the beam pairs are globally nulled: $\sum_{(i,j)} \psi_{\mathrm{OPD}(i,j)} = 0$. The closure phase, noted hereafter with Ψ, is then

$$\Psi = \sum_{(i,j)} \Phi_{(i,j)} = \sum_{(i,j)} \Phi_{*(i,j)} + \phi_{t(i,j)}. \tag{9}$$

A way to completely calibrate the instrumental effect $\sum \phi_{t(i,j)}$ would combine the techniques of closure phase, colour-differential phase and spatial modulation. The latter consists in commuting the interfering beams prior to their combination (Petrov et al. 2003, and Section 5.4). The precision of the closure phase measurement would then be limited only by the fundamental noise on the astrophysical term $\sum_{(i,j)} \phi_{t(i,j)}$.

3.4 Fundamental noises

We call 'fundamental noises' the sources of noise which cannot be reduced for a given instrumental setup, namely the photon noise, the background thermal noise and the detector readout noise. Let us first examine the effect of the noise on the measured phase, which has been analysed by Petrov (1989) and Chelli & Petrov (1995a). A correct approximation is to consider that the Gaussian error on the phase measurement at a given spectral frequency u is

$$\sigma_\Phi(u) = \frac{\sqrt{B_p^2(u)/2}}{M(u)}, \tag{10}$$

where $B_p(u)$ represents the level of noise and $M(u)$ the fringe signal, defined as the height of the fringe peak at the spatial frequency u. If

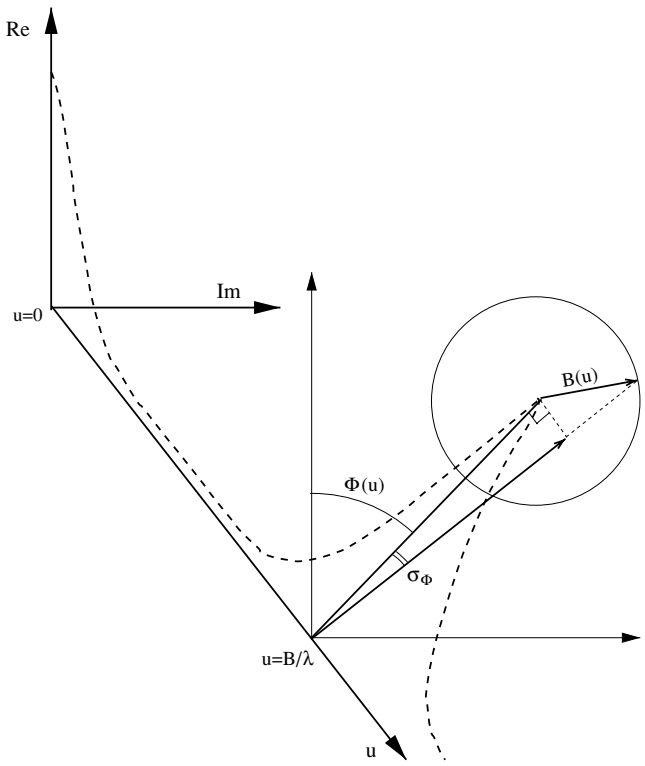

Figure 1. Illustration of the interferometric phase amplitude and noise. The phase Φ is defined as the argument of the fringe peak in the complex plane at the spatial frequency $u = \mathrm{B}/\lambda$. Some error σ_Φ on the measurement is introduced by the fundamental noise (projection of vector $\boldsymbol{B}$). In practice, the absolute phase is highly affected by unknown achromatic terms, so it is necessary to use relative measurements, e.g. the differential phase between two spectral channels (i.e. two different spatial frequencies).

$V(u)$ is the visibility contrast and N_i the level of flux brought by the aperture i to the fringe, then the amplitude of the fringe signal is

$$M(u) = V(u)\sqrt{N_i\, N_j}. \tag{11}$$

Let us assume hereafter that each of the n_{Tel} apertures equally yields a mean flux $\langle N\rangle$, and that there are no redundant baselines. Then, $M(u) = V(u)\,\langle N\rangle$.

The noise variance B_p^2 is the sum of the variances from the different sources of noise. The photon noise variance is equal to the total number of collected photons from the source: $N_* = n_{\mathrm{Tel}}\,\langle N\rangle$. The thermal noise variance is N_{th} (the number of photons from the thermal background), and the readout noise variance on n_{pix} pixels per frame and n_{f} frames can be written as $n_{\mathrm{f}}\, n_{\mathrm{pix}}\, \sigma_{\mathrm{RON}}$. Because the error on the signal is affected only by the perpendicular projection of the noise vector in the complex plane (see Fig. 1), the noise standard deviation is divided, on average, by a factor of $\sqrt{2}$. Then equation (10) is

$$\sigma_\Phi(u) = \frac{\sqrt{\left(N_* + N_{\mathrm{th}} + n_{\mathrm{f}}\, n_{\mathrm{pix}}\, \sigma_{\mathrm{RON}}^2\right)/2}}{V(u)\,\langle N\rangle}. \tag{12}$$

For the visibility, the error $\sigma_V(u)$ has a similar form, except for the fact that it is not normalized by the visibility itself, and that the factor $\sqrt{2}$ does not apply to the noise B_p^2, since we are interested

here in its amplitude and not in its phase. Therefore

$$\sigma_V(u) = \frac{\sqrt{N_* + N_{\rm th} + n_{\rm f}\, n_{\rm pix}\, \sigma^2_{\rm RON}}}{\langle N \rangle}. \quad (13)$$

For differential observables, the error includes uncertainties from both the studied spectral channel λ_i and the reference channel $\lambda_{\rm ref}$. If the reference quantity is integrated over a much wider band, as we suppose to be the case, the latter can be neglected in the first approximation.

Also, when observing relatively bright sources (typically $K = 5$ for the present application), equations (12) and (13) may take different forms for the near-IR (AMBER) and for mid-IR (MIDI) observations at VLTI. The photon noise is largely dominant in the noise budget of AMBER; thus the error can be simplified by neglecting the readout and thermal noise terms:

$$\sigma_\Phi(u) = \frac{1}{V(u)} \sqrt{\frac{n_{\rm Tel}}{2\langle N \rangle}} \quad (14)$$

and

$$\sigma_V(u) = \sqrt{\frac{n_{\rm Tel}}{\langle N \rangle}}. \quad (15)$$

On the other hand, the thermal background noise is the main source of noise for MIDI. An empirical law gives the expected value for the relative error on the phase of MIDI, which is inversely proportional to the N-band brightness $10^{-m_N/2.5}$ of the source.

Let us now compare the error σ_Ψ on the closure phase signal and the error σ_Φ on the phase measurement from an individual baseline, taken from the array of baselines used for the closure phase. Here, we assume the photon noise is dominant in the error budget, as it should be in the case of AMBER triple-baseline measurements.

The error on closure phase is the quadratic sum of the errors from the individual interferometric phases. The relationship between the errors on the closure phase with three telescopes (obtained on a multiple beams recombiner such as AMBER) and on the single-baseline phase in the same conditions is then simply: $\sigma_\Psi = \sqrt{3} \times \sigma_\Phi$.

Moreover, it can be shown (from equation 27) that the amplitude of the astrophysical signal with the closure phase comprises between 0 and 2 times the amplitude of the single-baseline phase signal, depending on the interferometric resolution and on the positions of the baseline vectors relatively to the source. For a source resolved on all the three baselines, one can consider the mean value $\Psi \simeq \Phi$, as an order of scale. Also, the closure phase measurement 'costs' three single-telescope time units. For the same cost, two independent single-baseline phase measurements could be measured. So, the amount of observation time for acquiring the same amount of information differs by a global factor

$$t_\Psi = \sqrt{3}^2 \times 3\, t_\Phi = 6\, t_\Phi. \quad (16)$$

In other words, for a given signal-to-noise ratio and quantity of information, closure phase requires six times more telescope time than single-baseline phase measurement.

4 DIFFERENTIAL PHASE FOR ESPS

Let us first present the interferometric observables in the general case of a binary system, and then express how they depend on some parameters of an extrasolar planetary system (the flux ratio between planet and star, their angular separation, the orbital phase) and how they can be translated into estimates of the spectrum, inclination and mass. We simplify the formalism by presenting the equations of the interferometric observables at a single wavelength. The phase is defined with an unknown additional constant, noted k, which disappears in the colour difference with an appropriate reference wavelength.

We note, respectively, by $I_1(\lambda)$ and $I_2(\lambda)$ the monochromatic luminosity of the two binary components, separated by an angle $\boldsymbol{\rho}$. The angular origin is taken on the first component. We first assume that the spatial distribution of each component is independent of the wavelength, i.e. both objects appear as a disc of constant diameter, defined by a normalized function $O(\boldsymbol{\theta})$ and weighted by $I(\lambda)$. Consider the Fourier transform $I_O(\boldsymbol{w}, \lambda)$ of the brightness distribution in the plane of spatial frequency $\boldsymbol{w}\,(u, v)$ covered by a single-baseline interferometer, where the u-axis component is chosen along the interferometric baseline $\boldsymbol{B}$ and takes the value $\boldsymbol{u} = \boldsymbol{B}/\lambda$. Note C_i, the visibility contrast of each component at the considered spatial frequency. The 'coherent flux' is the product $C_i\, I_i$.

$$I_O(\boldsymbol{w}, \lambda) = C_1\, I_1 + C_2\, I_2\, [\cos(2\pi \boldsymbol{u} \cdot \boldsymbol{\rho}) + j \sin(2\pi \boldsymbol{u} \cdot \boldsymbol{\rho})]. \quad (17)$$

The fringe phase is the argument of $I_O(w)$:

$$\Phi_* = \arctan \frac{C_2\, I_2 \sin(2\pi \boldsymbol{u} \cdot \boldsymbol{\rho})}{C_1\, I_1 + C_2\, I_2 \cos(2\pi \boldsymbol{u} \cdot \boldsymbol{\rho})} + k \quad (18)$$

and the visibility is its normalized amplitude

$$V_* = \frac{\sqrt{C_1^2\, I_1^2 + C_2^2\, I_2^2 + 2 C_1 C_2\, I_1 I_2 \cos(2\pi \boldsymbol{u} \cdot \boldsymbol{\rho})}}{C_1\, I_1 + C_2\, I_2}. \quad (19)$$

4.1 Approximation with a faint planetary companion

In what follows, we consider the specific case where the secondary component is a planet, with luminosity noted to be $I_{\rm p} = I_2$. Its angular size is completely unresolved by current long-baseline interferometers; therefore we take $C_2 = 1$. The stellar component can be marginally resolved.[3] We note hereafter its visibility $C_{\rm s}$ and its luminosity $I_{\rm s}$. For the case of a 'Pegasi' planet, the estimation of the flux ratio between the planet and the star ranges from a few 10^{-5} to 10^{-4} in the J band, 10^{-4} to 10^{-3} in the K band and several 10^{-3} in the N band (see Section 5.1). For planets with larger orbital separations, these ratios are even smaller; thus the following assumption is also valid. Considering that $I_{\rm p}(\lambda)/[C_{\rm s}(\lambda)\, I_{\rm s}(\lambda)] \ll 1$, a first-order approximation of equation (18) can be made:

$$\Phi_*(\lambda) \approx \frac{I_{\rm p}(\lambda)}{C_{\rm s}(\lambda) I_{\rm s}(\lambda)}\, \sin(2\pi \boldsymbol{u} \cdot \boldsymbol{\rho}) + k. \quad (20)$$

Similarly, equation (19) can be approximated by

$$V_*(\lambda) \approx 1 - \frac{I_{\rm p}(\lambda)}{C_{\rm s}(\lambda) I_{\rm s}(\lambda)} \left[1 - \frac{1}{2} \cos(2\pi \boldsymbol{u} \cdot \boldsymbol{\rho})\right]. \quad (21)$$

A favourable point of the differential technique for observing ESPs comes from the high difference in temperature, and therefore in colour, between the stellar and the planetary components. This implies that their flux ratio may vary largely between different spectral channels. If the spectral coverage is wide enough, one or several spectral channel(s) in which the ratio is expected to be particularly low may be chosen as a reference $\lambda_{\rm ref}$ for the colour-differential

[3] Among the targets discussed hereafter, the typical angular diameter of the stars is 1 mas. For a baseline $B = 100$ m, this corresponds to a visibility contrast of about 0.65 in J band and 0.9 in K band.

measurement, so that the signal in the reference channel is negligible compared to the signal at other wavelengths. For instance, observing a 'Pegasi' EGP simultaneously in J, H and K bands with AMBER allows to take $\lambda_{\rm ref}$ in the J band, where the planet/star ratio and thus the phase signal is at least 10 times lower than in the K band. The differential quantities in equations (4) and (5) can then be approximated by $\Delta\Phi_*(\lambda, \lambda_{\rm ref}) \approx \Phi_*(\lambda)$ with $k = 0$, and $V_*(\lambda, \lambda_{\rm ref}) \approx V_*(\lambda)$.

4.2 Effect of the planetary phase

Just like the Moon phase, the orbital phase of the planet determines, for a given orbital configuration, the proportion of its apparent enlightened surface (i.e. the fraction of visible 'day' croissant) over the whole disc area. Let $\phi_{\rm p}$ be the average orbital longitude of the planet as seen from the observer (with the origin $\phi_{\rm p} = 0$ at the maximum apparent separation), and i the inclination of the orbital plane with respect to the observer's line of sight. We define the ratio of the apparent 'day' surface over the total disc area as

$$P = \frac{1}{2}(1 + \sin\phi_{\rm p} \sin i). \tag{22}$$

The non-irradiated (i.e. 'night') side may also contribute to the total observed flux from the planet. Let c be the ratio of the brightness per surface unit between the night and the day sides. Depending on the wavelength and the circulation of energy in the atmosphere between the two sides, c might range from 0 (in the case where the flux contribution from the night side is null) to 1 (if the day and night parts are equally bright). We consider, here, only the thermal emission of the planet (which is clearly dominant in the IR flux budget of hot EGPs) and also assume that the effective temperature in either the bright or the dark area is homogeneous (i.e. each side emits isotropically over a semisphere). The ratio of the observed flux compared to a full 'day' disc is

$$P_{c(\lambda)} = P + c(1 - P) = \frac{(1 + c) + (1 - c)\sin\phi_{\rm p} \sin i}{2}. \tag{23}$$

The apparent flux received from the planet is then $P_{c(\lambda)}\, I_{\rm p}(\lambda)$, where $I_{\rm p}$ is the flux when the planet is viewed face-on as a full disc. In fact, the ratio c can be heavily constrained from theoretical studies. Models on atmospheric circulation (Showman & Guillot 2002) predict that the difference of temperature between the night and day sides of 'Pegasi' planets is about 400 K. Assuming a global effective temperature of 1000 K, this means a flux ratio c of about 1/100 in K band, and 0.4 at 10 μm. In the near-IR, the contribution from the night side yields a chromatic variation below the expected precision of the measurements (estimated further in this paper), and therefore we will consider $c \approx 0$ and $P_c \approx P$ in that case. The spectral shift due to Doppler effect should also be taken into account. It is shown to be negligible in the present case.[4]

4.3 Resolution and amplitude of the interferometric phase and closure phase

Note $\alpha(\lambda) = I_{\rm p}(\lambda)/[C_{\rm s}(\lambda)\ I_{\rm s}(\lambda)]$, the ratio between the coherent fluxes from the planet when viewed face-on and from the star. If we include the planetary phase factor, equation (20) becomes

$$\Phi_*(\lambda) = P_{c(\lambda)}\, \alpha(\lambda) \sin(2\pi \boldsymbol{u} \cdot \boldsymbol{\rho}) + k. \tag{24}$$

For a given wavelength, the maximum amplitude $\Phi_{\rm max}$ of the phase along the orbital motion follows two distinct regimes, depending on whether the argument $2\pi \boldsymbol{u} \cdot \boldsymbol{\rho}$ reaches $\pi/2$ or not. Let $(\boldsymbol{u} \cdot \rho)_{\rm max}$ be the maximum of the scalar product $\boldsymbol{u} \cdot \boldsymbol{\rho}$ along the orbit. If $(\boldsymbol{u} \cdot \rho)_{\rm max} \geqslant 1/4$, the system is resolved and the phase is represented as a periodic function of amplitude $\Phi_{\rm max}(\lambda) \approx P_{c(\lambda)}\, \alpha(\lambda)$. Alternatively, if $(\boldsymbol{u} \cdot \boldsymbol{\rho})_{\rm max} < 1/4$, the system is not interferometrically resolved, and the maximum phase is

$$\Phi_{\rm max}(\lambda) = P_{c(\lambda)}\, \alpha(\lambda) \sin[2\pi(\boldsymbol{u} \cdot \boldsymbol{\rho})_{\rm max}]. \tag{25}$$

If, for lower projected angular separation, $\boldsymbol{u} \cdot \boldsymbol{\rho}$ gets smaller below the resolution limit, the phase tends asymptotically towards a linear expression. It is then related to the photocentre vector ϵ_*, i.e. the barycentre of the star+planet brightness distribution:

$$\lim_{\boldsymbol{u}\cdot\boldsymbol{\rho}\to 0} \Phi_*(\lambda) = 2\pi\alpha(\lambda)\boldsymbol{u} \cdot \boldsymbol{\rho} = 2\pi/C_{\rm s}\, \boldsymbol{u} \cdot \boldsymbol{\epsilon}_*. \tag{26}$$

As for the closure phase of an EGP target, it is, according to equations (9) and (24),

$$\sum_{(i,j)} \Phi_{(i,j)}(\lambda) \approx \alpha(\lambda)\, P_{c(\lambda)} \sum_{(i,j)} \sin[2\pi \boldsymbol{u}_{(i,j)} \cdot \boldsymbol{\rho}]. \tag{27}$$

The sine function can be decomposed in terms of first order and of higher order of its Taylor expansion. Then the sum becomes

$$\sum_{(i,j)} \sin[2\pi \boldsymbol{u}_{(i,j)} \cdot \boldsymbol{\rho}] \approx 2\pi\left\{\sum_{(i,j)} \boldsymbol{u}_{(i,j)} \cdot \boldsymbol{\rho} + \sum_{(i,j)} o\left[(\boldsymbol{u}_{(i,j)} \cdot \boldsymbol{\rho})^3\right]\right\}, \tag{28}$$

where $o[(\boldsymbol{u}_{(i,j)} \cdot \rho)^3]$ groups the third and higher order terms. The sum of the first-order terms is null because it can be factorized by $\boldsymbol{\rho}$, and the spatial frequencies $\boldsymbol{u}_{(i,j)} = \boldsymbol{B}_{(i,j)}/\lambda$ is null on the closed loop of the baselines. If the system is non-resolved, the closure phase signal decreases fast with $\sum o[(2\pi \boldsymbol{u}_{(i,j)} \cdot \boldsymbol{\rho})^3]$ as $\boldsymbol{u}_{(i,j)} \cdot \rho$ gets smaller. This trend is to be compared with the decrease of non-resolved phase from a single baseline (equation 26), which varies with $\boldsymbol{u} \cdot \boldsymbol{\rho}$ on the first order. Non-resolution is therefore more critical when measuring a closure phase. Nearby hot EGPs such as 51 Peg (with a separation <5 mas) are partially resolved and could be observed by closure phase with VLTI in the near-IR (the interferometric resolution with AMBER being ≈4 mas in K band), but are too unresolved to give a measurable signal with a VLTI array at 10 μm (e.g. the Apres-MIDI project, see Lopez et al. 2003, with a resolution of ≈20 mas).

4.4 Determination of the planetary spectrum from the interferometric phase

Thanks to the photometric channels offered by the VLTI instruments, the spectroscopic data can be acquired at the same spectral resolution and simultaneously with the interferometric data. We therefore have the star+planet flux

$$I(\lambda) = I_{\rm s}(\lambda) + I_{\rm p}(\lambda). \tag{29}$$

The spectrum $I_{\rm p}(\lambda)$ can be determined by combining either the interferometric phase (equation 24) or the visibility (equation 21) with the spectroscopic measurement $I(\lambda)$. (In the following equations, we omit the dependence of the variables with wavelength λ, for a more simple notation). The planetary flux as a function of the phase is

$$I_{\rm p} = \frac{I\, C_{\rm s} \Phi}{C_{\rm s}\Phi + P_c \sin(2\pi \boldsymbol{u} \cdot \boldsymbol{\rho})}. \tag{30}$$

[4] For a 'Pegasi' planet, the measured Doppler shift of the star $\delta\lambda_*$ is typically a few 10^{-7} μm at 2 μm. Assuming a planet/star mass ratio equal to $M_{\rm Jup}/M_{\rm Sun} \approx 10^{-3}$, this yields a shift of about $\delta\lambda_{\rm p} = 10^{-4}$ μm on the planetary spectrum. This is far below the available spectral resolution capability at the VLTI. We can therefore neglect the Doppler shift.

As a function of the visibility, the planetary flux is

$$I_{\rm p} = \frac{I\,C_{\rm s}\left[1-\frac{1}{2}\cos(2\pi \boldsymbol{u}\cdot\boldsymbol{\rho})-V\right]}{1-\frac{1}{2}\cos(2\pi \boldsymbol{u}\cdot\boldsymbol{\rho})+C_{\rm s}\left[1-\frac{1}{2}\cos(2\pi \boldsymbol{u}\cdot\boldsymbol{\rho})-V\right]}. \quad (31)$$

The primary unknowns above are contained in the angular vector $\boldsymbol{\rho}$. Since each of the two equations above contains a complementary trigonometric function of $\boldsymbol{u}\,.\,\boldsymbol{\rho}$, the scalar product can be determined by combining them. That yields the spectrum as a function of $V(\lambda)$ and $\Phi(\lambda)$. This assumes, though, that both the differential phase and the visibility can be measured at the goal precision. Also, from just one baseline (i.e. a unique $\boldsymbol{u}$), the vector $\boldsymbol{\rho}$ (and subsequently the planetary orbital elements) is still undetermined.

We develop hereafter a solution where both the spectrum and the angular vector $\boldsymbol{\rho}$ can be obtained by a single-time measurement of just one differential observable along two baseline directions. We choose to give the formalism as a function of the phase $\Phi(\lambda)$, although it could as well be expressed as a function of the visibility. The orbital elements for a circular orbit[5] appear explicitly into the scalar product $\boldsymbol{u}\cdot\boldsymbol{\rho}$:

$$\boldsymbol{u}\cdot\boldsymbol{\rho}(t) = \frac{B}{\lambda}\frac{a}{\rm d}[\cos\theta\sin\phi_{\rm p}(t)+\cos i\sin\theta\cos\phi_{\rm p}(t)], \quad (32)$$

where a is the semimajor axis, d the distance between the planet and the observer, $\phi_{\rm p}(t)$ the orbital phase, θ the angle between the baseline direction and the major axis of the apparent ellipse covered by the inclined orbit. θ is directly related to the longitude of the ascending node Ω and to the orientation of the baseline. Since this method does not aim at detecting new planets, but rather at getting the spectrum, inclination and mass of planets previously detected by RV surveys, the orbital parameters a and $\phi_{\rm p}(t)$ as well as the lower mass estimate $M\sin i$ are supposed to be provided from the RV data. Also, we assume that the stellar distance d is known (from the *Hipparcos* parallax the precision on d is typically 1 per cent for our targets).

The CDI observations can be made at the maximum star–planet apparent separation, i.e. at the orbital phase $\phi_{\rm p}=\pi/2$ where $\rho_{\max}=a/d$. In that configuration, half of the planetary disc appears irradiated from the observer's point of view, and $P_c=(1+c)/2$. The parameter of inclination i then disappears from equation (32) and only the orientation angle θ remains unknown, so equation (24) can be written as

$$\Phi_{(\phi_{\rm p}=\pi/2)} = \frac{1+c}{2}\,\alpha(\lambda)\sin\left(2\pi\frac{B}{\lambda}\frac{a}{d}\cos\theta\right). \quad (33)$$

Angle θ is obtained from the ratio between the differential phase measurements along two different baseline directions, at that position $\phi_{\rm p}=\pi/2$ of maximum separation. For instance, if the baselines (noted as $\boldsymbol{B}_1$ and $\boldsymbol{B}_2$) are perpendicular and have the same length, the angle θ with respect to the direction of $\boldsymbol{B}_1$ is

$$\theta = \arctan\frac{\arcsin\Phi_{\boldsymbol{B}_2}}{\arcsin\Phi_{\boldsymbol{B}_1}}. \quad (34)$$

As $\boldsymbol{u}\cdot\boldsymbol{\rho}$ is determined for that position, the error $\sigma_{I_{\rm p}}$ on the planetary spectrum can be estimated by deriving equation (30) as a function of the relative errors σ_Φ on the phase and σ_I on the total spectrum:

$$\sigma_{I_{\rm p}} = \frac{C_{\rm s}(\Phi\,\sigma_I + I\,\sigma_\Phi)[C_{\rm s}\Phi + P_c\sin(2\pi\boldsymbol{u}\cdot\boldsymbol{\rho})] + I\,C_{\rm s}\,\Phi\,\sigma_\Phi}{[C_{\rm s}\,\Phi + P_c\sin(2\pi\boldsymbol{u}\cdot\boldsymbol{\rho})]^2}. \quad (35)$$

Which of the terms $\Phi\,\sigma_I$ or $I\,\sigma_\Phi$ is dominant in the error budget? For the typical case of a hot EGP around a nearby star, we expect (see Section 5.2) that the signal-to-noise ratio on the phase Φ/σ_Φ will be of the order of a few tens or less. On the other hand, the error on the spectrum is dominated by the photon noise of the star, so that $s/\sigma_s=\sqrt{N_*}$, i.e. several thousands for a magnitude five star observed during more than 1 h at a low spectral resolution. Therefore, $I\,\sigma_\Phi \gg \Phi\,\sigma_I$, so $\sigma_{I_{\rm p}}$ is strongly dominated by the phase error term. Also, equations (35) and (30) can be simplified by the fact that $C_{\rm s}\,\Phi \ll P_c\sin(2\pi\boldsymbol{u}\cdot\rho)$. The ratio between these two equations yields that the relative error on the spectrum is approximated by the relative error on the phase:

$$\sigma_{I_{\rm p}}/I_{\rm p} \approx \sigma_{\Phi_{\rm p}}/\Phi_{\rm p}. \quad (36)$$

4.5 Determination of the orbital inclination and planetary mass

Here, we assume that the flux contribution from the non-irradiated side is negligible, i.e. that the parameter of planetary phase is $P_c=(1+c)/2$. As mentioned in Section 4.2, this statement should be true for giant planets with tidally locked orbits observed in the near-IR wavelengths. Suppose that the differential phase is first measured along two baselines at the orbital phase $\phi_{\rm p}=\pi/2$, as described in the previous paragraph, thus yielding the flux ratio, the orientation angle θ and the scalar product $\boldsymbol{u}\cdot\rho_{\pi/2}$. A second set is measured along the same baselines a quarter of an orbit further, at the orbital phase $\phi_{\rm p}=\pi$ where $\rho_\pi=\rho_{\pi/2}\cos(i)$ and $P_c=(1+\sin i)/2$. The inclination may be determined by combining equations (24) and (32). We can explicit α from equation (33) with $c=0$, and separate the terms which depend on i from the others in order to get the form $f(i)=g(\Phi_\pi,\Phi_{\pi/2})$:

$$(1+\sin i)\sin(2\pi\boldsymbol{u}\cdot\boldsymbol{\rho}_{\pi/2})\tan\theta\cos i = \sin(2\pi\boldsymbol{u}\cdot\boldsymbol{\rho}_{\pi/2})\frac{\Phi_\pi}{\Phi_{\pi/2}}. \quad (37)$$

There is no straightforward literal solution for the equation above, but its roots can easily be resolved numerically. The error on the inclination can be expressed as a function of the error on the phase using the differential form of each side. If we neglect the error made on $\rho_{\pi/2}$ from RV data and parallax, the derivative of the left-hand term is $\mathrm{d}f=(\delta f/\delta i)\,\mathrm{d}i$. The right-hand term is derived with respect to the error $\mathrm{d}\,\Phi=\sigma_\Phi$ on the two phase measurements, which, in a first-order approximation, are here supposed to be independent of the orbital position since the stellar photon noise strongly dominates: $\sigma_{\Phi_\pi}\approx\sigma_{\Phi_{\pi/2}}$ and $\Phi_\pi\approx\Phi_{\pi/2}$. Then, the error $\sigma_i=\mathrm{d}i$ on the inclination is

$$\sigma_i = 2\,\frac{\sin 2\pi\boldsymbol{u}\cdot\boldsymbol{\rho}_{\pi/2}}{\delta f/\delta i}\frac{\sigma_{\Phi_{\pi/2}}}{\Phi_{\pi/2}}. \quad (38)$$

From this, the error on the planetary mass M is obtained simply. If we note $K=M\sin i$, the lower estimate of the mass from RV data, then

$$\sigma_M = \frac{K}{\tan i}\sigma_i. \quad (39)$$

The errors on i and M are higher for the particular values of i where $\delta f/\delta i$ approaches zero. Such effect is smoothened by using a

[5] In the general case, not treated here, of a non-circular planetary orbit, the additional parameters of eccentricity e and the argument of perihelion ω would appear in equation (32). These parameters are in principle also known from RV measurements, so they are not additional unknowns but just add complexity to the equations presented here.

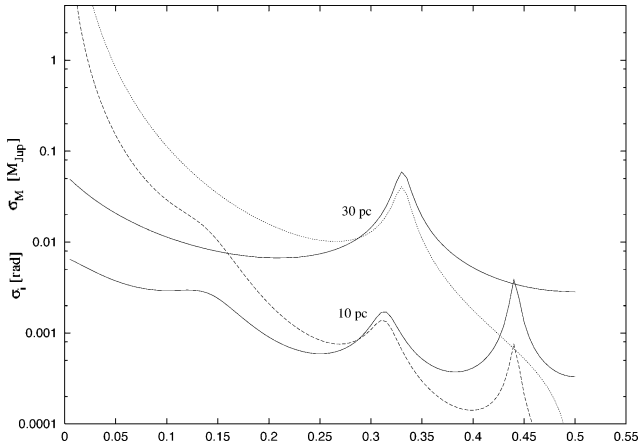

Figure 2. Achievable precision from the photon noise on the orbital inclination i (full lines) and the planetary mass M (dashed and dotted lines) as a function of i, assuming a planetary mass $M = 1.4\,M_{\rm Jup}$ and an orbital distance of 0.05 au around a solar-type star at a distance of 10 pc (top curves) and 30 pc (bottom curves). The input noise on the differential phase signal corresponds to 5 h of exposure time on 2 UT with AO, in K band at a low spectral resolution. The errors on i (and thus on M) rise sharply for certain spatial frequencies. This effect is smoothened by considering several (here seven) spectral channels.

weighted estimator of σ_i over several spectral channels, i.e. several spatial frequencies $u_i = B/\lambda_i$. Fig. 2 shows some typical results, as a function of the inclination. When observing over a few hours, a close-in EGP ($a \approx 0.05$ au) at a distance up to a few tens of parsecs, the error on the inclination i is lower than 0.1 rad for most values of i. The error on the mass is lower than 0.1 Jupiter mass, except if the inclination tends towards low values where, for a given $M \sin i$, the error on M increases fast with $1/\tan i$.

5 ESTIMATES OF OBSERVABILITY

5.1 Assumption on the astrophysical source

For estimating the potential of differential interferometry for ESPs observation, we considered a selection of about 70 objects with short orbital distance, among the 170 ESPs detected so far by RV (from the catalogue established by J. Schneider).[6] Only the objects ranging below $M \approx 13\ M_{\rm Jup}$, often considered as the deuterium combustion critical mass and a limit for brown dwarf classification, are investigated hereafter; since brown dwarfs have a high intrinsic thermal emission independent of their distance to the star, they would be more favourable candidates for the observation using the differential phase method (Ségransan et al. 2000). The fluxes of the EGPs are modelled using some synthetic spectra furnished by T. Barman, following the method described by Barman et al. (2001). These synthetic spectra were calculated for an irradiated 1-Jupiter mass EGP orbiting at various distances (0.05, 0.08, 0.1, 0.2, 0.3, 0.5 and 1 au) around a G2 star. We use the model of a 'condensed' atmosphere, which appears far more realistic than the 'dusty' or 'blackbody' (BB) model for the case of hot EGPs[7] on which we focus hereafter. A spline interpolation of these synthetic spectra to the actual orbital distance of the considered EGP is computed. The planetary flux is then obtained by scaling its emitted radiation to the estimated surface of the disc, using an empirical fit taken from Guillot's mass–radius computations for a dozen of strongly irradiated EGPs (Guillot 1999). It predicts a radius decreasing from about 1.5 $R_{\rm Jup}$ for the most close-in and least-massive EGPs to about 1.05 $R_{\rm Jup}$ for 10 Jupiter-mass planets. We coarsely estimate the planetary mass by adding to $M \sin i$ (given by velocimetry measures) a mean factor of 30 per cent accounting for the unknown inclination term. Due to the various uncertainties on mass, age and input physics, the fitted law on the radius contains a relative error of typically ± 15 per cent. That means an error of ± 30 per cent rms on the planetary fluxes, and the same error on the signal-to-noise ratio estimate. This translates in a large error of ± 60 per cent on the estimated exposure time for a given signal-to-noise ratio.

5.2 Results of the modelling

Fig. 3 shows an example of the amplitudes of interferometric phase with VLTI and the corresponding levels of fundamental noise over a long exposure, for a 51 Peg-like system (orbital separation of 0.05 au) and a giant planet at separation 0.08 au, both at a distance of 10 pc. The amplitude of the *differential* phase in the J, H and K bands of AMBER is estimated to range between several units and a few tens above the noise level, depending on which spectral channels are compared with each other. For MIDI, the colour-differential measurement is much less favourable due to the flatness of the phase as a function of wavelength; the signal-to-noise ratio of the differential phase is of the order of one unit, in this case.

Table 1 lists, for a number of known EGPs, the estimated observation time $t_{3\sigma}$ needed to get a signal-to-noise ratio of 3 on the planetary flux in each spectral channel.

The most favourable targets for CDI are the EGPs with the shortest orbital distance (around 0.05 au or less). The explanation for this is simple. When the distance a decreases, the stellar flux impinging the planet increases faster (as $1/a^2$), and the overall signal increases as well. For a given orbital distance, nearby and bright stars are obviously favoured, since their photon noise is lower and the angular separation is larger. For such nearby 'Pegasi' objects, $t_{3\sigma}$ may be as small as a few tens of minutes with AMBER/VLTI in the full K band. (If we considered, instead of a condensed model, the pessimistic assumption of a BB emission, $t_{3\sigma}$ would be a couple of hours for these objects.) These results can be extrapolated to the medium-resolution mode ($R = 1500$) offered by AMBER, by applying a factor of $1500/35$ on $t_{3\sigma}$: each of the three most favourable targets could barely be observed at medium resolution within a full night with a signal-to-noise ratio of 3. In the low-resolution mode $R = 35$, a dozen of targets would yield a significant signal-to-noise ratio in K band within a full night, according to the synthetic spectra assumption. Their orbital distances range between $a = 0.038$ and 0.07. The H band, and even more the J band, offers a lower signal for an equivalent amount of fundamental noise, and only a handful of objects could be observed within a few hours in these bands.

[6] See http://www.obspm.fr/encycl/catalog.html

[7] Barman et al. (2001) have investigated both models of 'condensed' and 'dusty' planetary atmospheres. For planets with orbital distance $a < 0.15$ au, the authors have only used the hypothesis of a condensed atmosphere, which is favoured in the case of strongly irradiated planets. 'Condensed' means here that all the dust has been removed from the atmosphere by gravitational settling, thus spectral absorption features appear deeper. On the opposite case, the dusty models assume that the dust and grain particles remain in the atmosphere and contribute to diffuse the light. For comparison, we also considered an improbable BB radiation model, taken as the lowest and smoothest (i.e. most pessimistic) limit for the flux of our targets in the near- and mid-IR range.

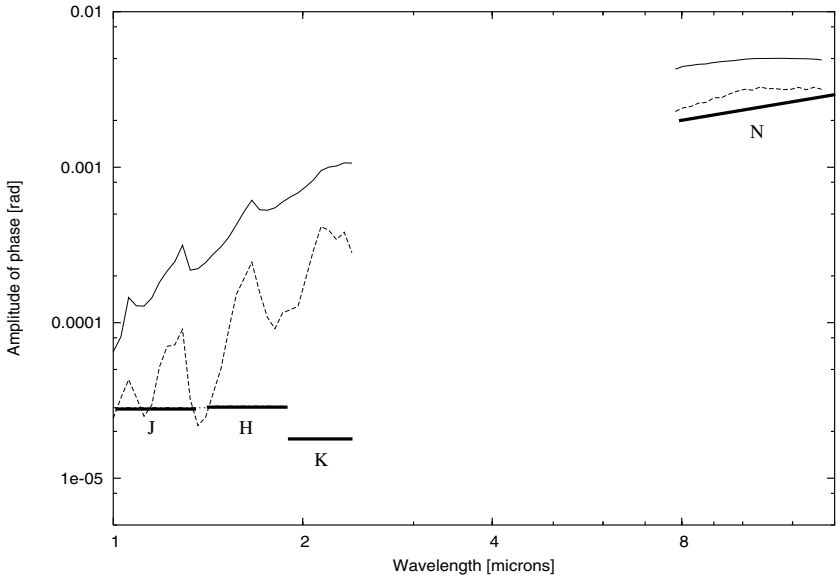

Figure 3. Estimated amplitude of interferometric phase $\phi(\lambda_i)$, as a function of wavelength at a low spectral resolution, for a hypothetical Jupiter-mass planet at an orbital separation of 0.05 au (full line) or 0.08 au (dotted line) around a G2 star located at 10 pc. The signal is to be compared with the levels of fundamental noise (thick lines) corresponding to 5 h of exposure time on the AMBER and MIDI instruments of the VLTI (assuming two 8-m telescopes with AO and a spectral resolution $R = 35$).

Table 1. Estimated potential of colour-differential interferometric observation on some known EGP candidates, in *H* and *K* bands (AMBER/VLTI) and in *N* band (MIDI/VLTI). The effective integration time $t_{3\sigma}$ for obtaining a signal-to-noise ratio of 3 in each spectral channel, with a spectral resolution $R = 35$, is indicated in hours (up to a limit of 30 h). It does not include the calibration exposures and the overheads (in particular the chopping, for observations made in *N* band). We used synthetic spectrum models from Barman et al. (2001) for the planetary flux (see text for details). Note that the error on $t_{3\sigma}$ is large (±60 per cent), mostly due to the unknowns on the planetary mass and age.

EGP	V (mag)	Sp. type	a (au)	$M \sin i$ ($M_{\rm Jup}$)	ρ (mas)	$t_{3\sigma}$ (h) H	K	N
tauBoo	4.5	F7	0.046	3.8	2.88	2.0	0.2	7.8
upsAnd1	4.63	F7	0.059	0.71	4.25	4.4	0.3	3.4
51 Peg	5.49	G2	0.05	0.47	3.16	4.2	0.3	7.2
HD75289	6.35	G0	0.046	0.42	1.54	12.8	0.8	>30
H179949	6.25	F8	0.045	0.84	1.63	14.5	1.0	>30
HD46375	7.94	K1	0.041	0.249	1.19	>30	2.3	>30
H217107	6.16	G8	0.07	1.28	3.45	>30	2.5	>30
HD83443	8.23	K0	0.038	0.35	0.84	>30	4.7	>30
H187123	7.79	G5	0.042	0.52	0.81	>30	5.0	>30
H209458	7.65	G0	0.045	0.69	0.93	>30	6.9	>30

The signal-to-noise ratio also drops strongly when observing the same object in *N* band (MIDI), where the thermal noise is high. Only a very few number of targets (all of which with $a < 0.06$ au, around very nearby stars) might be detected with MIDI within a nighttime.

5.3 Astrophysical noises

Some astrophysical sources other than the ESP might affect the colour-differential detection. If we assume that the field of view is not polluted by some other sources of light in the foreground or background of the star, the astrophysical noises include the stellar rotation and non-radial stellar oscillations, the stellar activity (spots and faculae) and the exozodiacal light.

Since the star of any extrasolar planetary system can be considered as mostly unresolved, the angular effects of stellar rotation, non-radial oscillations and stellar activity will produce on the fringe pattern a differential phase proportional to the displacement of the stellar photocentre $\epsilon(\lambda)$, as stated in equation (26).

5.3.1 Stellar rotation

Several authors (Lagarde 1994; Chelli & Petrov 1995b) have computed the photocentre displacements produced by a rotating star possibly affected also by radial or non-radial oscillations. Their results can be summarized by saying that the maximum photocentre displacement $\Delta\epsilon_{\rm max}(\lambda_l, \lambda_{\rm ref})$, measured between wavelength λ_l of an absorption line and a reference wavelength $\lambda_{\rm ref}$ taken in the continuum, is given by

$$\Delta\epsilon_{\rm max}(\lambda_l, \lambda_{\rm ref}) \approx A(1-p)\frac{R_*}{d_*}\frac{V_{\rm rot}\sin i + V_{\rm nr}}{\Delta V_{\rm line}}, \quad (40)$$

where R_* is the stellar radius, d_* the distance, $V_{\rm rot}\sin i$ the rotation velocity and $V_{\rm nr}$ the amplitude of the velocity fluctuations due to non-radial oscillations. The line is described by its depth p (with $0 < p < 1$), defined without stellar rotation and instrument broadening, and by its equivalent width $V_{\rm line}$, which combines the natural width of the line and the effect of the instrument spectral resolution. The factor A is an integration factor depending on the stellar limb darkening and on the exact line profile. For all usual set of parameters, $0.1 < A < 0.2$, and we will take here $A = 0.15$. For any spectral resolution smaller than $R = 10\,000$, the measured line width will be dominated by the instrument profile and $V_{\rm line} = c/R$. For stars close to the solar type, the typical $V_{\rm rot}\sin i$ is a few km s^{-1}. $V_{\rm nr}$ is smaller than 100 m s^{-1} and can therefore be neglected with regard to the rotation velocity. Among the targets listed in Table 1, the strongest rotation effect is expected on τ Bootis, with $V_{\rm rot}\sin i = 14$ km s^{-1},

$p = 0.5$ and $R_*/d_* \approx 1$ mas. For baseline $B = 100$ m, wavelength $\lambda = 2$ μm and the lowest resolution of AMBER $R = 35$, we get

$$\Delta\epsilon_{\max}(\lambda_l, \lambda_{\rm ref}) = 1.2 \times 10^{-7} \text{ arcsec}$$

and

$$\Phi_{\rm rot}(\lambda_l, \lambda_{\rm ref}) = 1.8 \times 10^{-4} \text{ rad}.$$

This phase value is comparable to the signal expected from a 'Pegasi' planet displayed in Fig. 4. It must therefore be measured. A possible solution is to use the higher spectral resolution of AMBER ($R = 12\,000$) to measure the phase across one line [$\Phi_{\rm rot}(\lambda_l, \lambda_{\rm ref}] \approx 0.06$ rad, signal-to-noise ratio ≈50 for 30 min of integration time), in order to obtain the exact diameter of the star and the position angle of its rotation axis. These values can then be combined with measured spectra to compute the effect of stellar rotation at low resolution. In addition, the position angle of the rotation axis gives an interesting clue on the position angle of the planetary orbit, and can eventually be compared with the actual orientation of the orbital plane.

5.3.2 Stellar spots

For solar-type star, the typical total size of the spots may represent about 1 per cent of the disc. The theoretical computation by Aigrain, Favata & Gilmore (2004) shows important differences between stars of various type and age, but photometric variations in white light stay lower than a few 10^{-5} over a few hours. This order of scale seems consistent with the data gathered by VIRGO/SOHO for the sun: after substracting the long-term drift, we computed a relative standard deviation due to solar activity of about 2×10^{-5} over a few hours in the red band. The relative variations of photometry are expected to be significantly lower in the near-IR range than at shorter wavelengths or over the whole integrated spectrum. We therefore take 10^{-5} as an estimate of the variations in *J* band. Assume, in the most pessimistic case, that the sunspot's distribution is non-symmetrical with respect to the rotation axis and is located at the maximum possible separation of the photocentre (i.e. almost one stellar radius from the disc centre). The resulting shift of interferometric phase is then lower than the level of noise over a few hours of integration; e.g. about 7×10^{-6} rad for a star at 10 pc. The stellar spots can therefore be considered to have a negligible effect.

5.3.3 Exozodiacal light

Exozodiacal light is the scattered diffusion of the stellar light by the surrounding dust. Its distribution is in principle symmetrical around the star, so its effect on the displacement of the photocentre is only an additional weight that lowers the effect of the asymetrical distribution due to the planet. In a general case, the quantity of exozodical light is largely unknown, as it depends on the (hypothetical) history of collisions in the planetary system. We consider the only available data, the zodiacal light in our Solar System, taken from the estimated dust temperature according to the *COBE* model. The emission from the dust is much higher at 10 μm than at shorter wavelength, and strongly decreases with the orbital radius, from about 10^4 MJy sr^{-1} at 0.01 au to 20 MJy sr^{-1} at 1 au, for a solar-like system located at 10 pc. In the most pessimistic configuration of a face-on zodiacal disc, the integration of the 10-μm emission between 0.01 and 1 au gives a relative weight of about 10^{-5} rad. That is, a factor of about 10^{-2} below the noise level in *N* band. Although it would be hazardous to extrapolate our knowledge of the Solar System's zodiacal light to other stars, the large margin below the detection levels even for the most pessimistic case indicates that exozodiacal light is unlikely to bias the measurements.

5.4 Instrumental and atmospheric chromatic effects

From the present study, it appears that if the measurements were affected only by the fundamental noises and if we properly treat the astrophysical phenomena, the goal of doing hot EGP spectroscopy with the VLTI is achievable. This assumes, though, being able to measure differences of phase ranging from a few 10^{-5} to 10^{-4} rad. In terms of stability, this is a very challenging technical goal: up to now, differential interferometry with GI2T allowed to approach a precision of 10^{-2} rad (Vakili et al. 1994) and the similar technique of differential speckle interferometry showed results in the 10^{-3} rad range (Sánchez et al. 1997). We have therefore to gain at least one order of magnitude in the control on the differential phase stability.

In Petrov et al. (2003), we describe a systematic analysis of all instrumental and atmospheric contributions to the differential phase. Due to the single-mode fibre spatial filtering, the effects occurring before the fibres produce only temporal variations of the chromatic OPD. These variations are due to instrumental factors (changes in the difference of temperature between the fibres, combination of residual beam motions through imperfect optical elements,. . .) and the chromatic dispersion of the air (in the open atmosphere and in the interferometric tunnels) where the refractive index depends on the local properties of temperature, pressure and humidity. After the fibres, additional errors on the chromatic phase may come from the beam combination and detector defects, together with chromatic variations of the spectrograph point spread function (PSF). Also, a significant 'chromatic-like' effect might come from the instantaneous (achromatic) piston in each frame combined to the fact that the spectral channels on the detector are not read exactly at the same time. This can be corrected using a specific data processing and will eventually be cancelled when a fringe tracker is operational.

Overall, we estimate that this could produce phase variations of several 10^{-2} rad over the bandwidth in the near-IR, in a time-scale of a few minutes. Our strategy to overcome these effects has several angles.

(i) By design and construction, the instrumental effects have been reduced and made slow enough to be eliminated by an internal modulation at typical 0.02-Hz frequency (Vannier et al. 2003). This modulation consists in regularly exchanging two of the beams feeding AMBER, using a dedicated Beam Commuting Device (BCD). The atmospheric and astrophysical terms are then inversed while the instrumental terms remain constant, assuming the modulation is fast enough. Instrumental effects can therefore be eliminated in the difference between measurements made with and without beam commutation.

(ii) The remaining variable chromatic terms come from atmospheric dispersion. Akeson, Swain & Colavita (2000) made measurements with Palomar Testbed Interferometer in the IR and found phase perturbations as large as a few 10^{-2} rad, which they interpreted as mainly due to variation of the thickness of water vapour in the two beams. The dominant effect of water vapour dispersion has been further analysed theoretically and quantified by Colavita et al. (2004), who found a similar amplitude on the resulting error of differential phase. In the mid-IR, these effects were recently measured with MIDI and discussed by Meisner & Le Poole (2003) and Tubbs et al. (2004). In the latter reference, the authors found the measurements to be in agreement with a model for the refraction of the air based on the HITRAN data base.

Since the spectral intervals used by the VLTI instruments are not affected by strong atmospheric lines, the dispersion over these intervals is fairly smooth with wavelength. In the near-IR, the difference in dispersion between the beams follows a known standard law, function of wavelength, multiplied by only two unknown variable parameters: the integrated thickness differences in dry air and in water vapour [see Ciddor (1996) for a detailed discussion on the dispersion law]. We estimate that these effects can be extracted from each exposure frame of the data set, the number of variable astrophysical and atmospheric unknowns being lower than the number of differential phase equations (Vannier et al. 2005a). An alternative (or complementary) possible way to monitor the dispersion law is to use a spectral channel where the astrophysical signal is known to be very low, such as at the beginning of the *J* band. In both the cases, a side effect of the removal of the continuous dispersion from the differential phase is that it might as well suppress part of the astrophysical signal which would have a similar shape in wavelength. Therefore, it might decrease the planetary continuum signal. And it remains to show in practice up to which extent the variations of the atmospheric dispersion due to changing conditions of the air during each exposure frame and between the science source and its calibrator star can indeed be monitored for correction.

(iii) The use of closure phase with three telescopes eliminates all the OPD terms, including the atmospheric ones, whatever is their amplitude. However, the beam combination and detector terms remain. They can be removed by commuting two of the three AMBER beams using the BCD. This produces the modulated closure phase, which is in principle independent of any atmospheric and instrumental effect. Nevertheless, the use of closure phase has a substantial cost in telescope time, as shown previously (Section 4.3).

Our observing plan can finally be summarized as follows. Use the colour-differential phases individually from three baselines (i.e. three telescopes), eliminate the instrumental effects by commuting the beams and try to suppress the atmospheric effects in the model fitting. If this is insufficient, we will use the modulated closure phase from the combination of the three baselines. We are quite confident that one of these steps will yield phase or closure phase chromatic variations close to the level set by the fundamental noises.

5.5 Current precision on AMBER

First tests of the stability of the differential and closure phase were performed during the first commissioning and advanced guaranteed time runs of AMBER (end of 2004). The extremely high accuracy needed for ESPs was not the first priority in these early phases of AMBER commissioning, and the following results have been obtained without Beam Commutation Device (which is currently being commissioned), without specific thermal insulation of the fibres and with a software and observing procedures not yet optimized for extreme accuracies. The corrections of the atmospheric longitudinal dispersion were not implemented. A very important factor is that the fringe tracker is not yet available; this implies using very short exposures and correcting the effects of the achromatic variations of the piston. The data of these early runs, as well as most recent BCD commissioning data, are still being processed as we write this, and a detailed discussion of the results would anyway go well beyond the scope and possible length of this paper. However, we summarize here the situation at the present time (2005 November). More information can be found in Vannier, Millour & Petrov (2005b) and Millour, Petrov & Vannier (2006).

We have observed calibrator stars at medium ($R = R$) and low spectral resolution ($R = R$). In both the cases, we analyse the temporal stability of the measurements in each spectral channel as a function of time as well as the statistical dispersion of the values as a function of wavelength, over several series of exposure frames, which are about 20 s long each, separated by about 1 min and therefore spanning over a total time of 5 min.

The medium resolution observations display differential phase measurements with a statistical dispersion of $\sigma = 8 \times 10^{-3}$ rad for 25 s of effective observations (twice the photon noise level), stable over a range of 15 min. The structures in the wavelength direction are up to 30 pixels (0.2 μm) in width, with amplitudes reaching 20×10^{-3} rad. They are stable over at least a few minutes. An important point is that these features appear also in the closure phase, with amplitudes comparable to, or larger than, the quadratic addition of the single-baseline structures. This indicates that they are not due to OPD but are rather produced by spatial filtering and detector defects. In medium resolution, they will be filtered down to typically 3×10^{-3} rad, which means that we still need to use the BCD to eliminate them.

In low resolution, the standard deviation of the differential phase measurements for each spectral channel and within each series of frames is typically $\sigma = 1.8 \times 10^{-3}$ rad (i.e. 1 μarcsec fringe displacement). This is less than two times the fundamental noise, computed from the measured flux and instrumental visibility. Over the total 5 min, we get $\sigma = 0.9 \times 10^{-3}$ rad, again very close to twice the photon noise. This shows that the different series of exposures is statistically independent on this time-scale. Therefore, in current conditions, the accuracy of 0.5×10^{-4} rad required for the spectroscopy of the most favourable 'Pegasi' planets could be reached with 1200 such frame series, i.e. 18 h of observation. With the planned improvement of the VLTI (less vibrations, reduced overheads), we can expect to multiply by two the number of usable frames, and to improve the average instrumental contrast by also a factor of 2 (i.e. an additional gain of a factor 4 in time). Then, from the point of view of fundamental signal-to-noise ratio, the observation of hot giant exoplanets would be achievable in about 2 h.

A fairly stable chromatic pattern appears on all the frame series, with a peak-to-valley amplitude of 10^{-2} rad between the spectral channels of the *K* band. This pattern varies typically by 10^{-3} rad between successive frame series, and these variations appear stationary over our 5-min time-span. They are due to a combination of variable atmospheric dispersion and instrumental effects, as mentioned in the previous section. We saw that the contribution produced in the instrument could in principle be calibrated by a Beam Commutation every minute down to at least 10^{-3} rad, and that the contribution due to atmospheric dispersion part could be fitted in each data frame (see Section 5.4). Then, only 2 h of observation would be necessary for the spectroscopy of the most favourable candidates.

At the moment, our closure phases are much noisier (typically $\sigma = 10^{-2}$ rad rms) than the individual differential phases, therefore we could not assess the contribution of detection effects to the differential phase wavelength pattern. This is due to the fact that we have too few frames with good fringes simultaneously on the three baselines. That specific effect should be corrected with only a fraction of the improvements currently in progress on the VLTI vibrations and photometric stability. With a larger proportion of simultaneous good-quality frames, the closure phase combined with beam commutation would be free of instrumental and atmospheric effects, and would also allow the observation of our best target in 2 h.

The differential visibility measurements in low resolution vary by only 4×10^{-3} rad with time within each frame series, but the

general slope of the curve changes dramatically between the successive series, leading to a variation of about 50×10^{-3} rad rms over 5 min. This variation is dominated by the changes in the achromatic piston jitter due to seeing and vibration fluctuations. Currently, we have no tool to correct this effect, except including an estimation of the exposure jitter in the model fitting, with an impact on the signal-to-noise ratio which cannot be estimated yet. So the differential visibility is currently not usable for very high precision applications. This situation will change very significantly when a fringe tracker is operational.

If none of the BCD, dispersion fit or closure phase correction works, we would have to use calibrators at least 20 min away in time, with an error dominated by the calibration of about 510^{-3} rad every 40 min. Thus, if we are strictly limited to the current situation, only a planet brighter than 10^{-3} times the star could be observable in a 20-h time with the Unit Telescopes. For that time, the first spectroscopy of a 'Pegasi' planet would still be worthwhile. We are nevertheless confident that a large part of the variable effects could be substracted or corrected, and that the necessary observational time will therefore be reduced significantly.

6 CONCLUSION

CDI on ground-based long-baseline interferometers with large apertures (such as the VLTI or the Keck Interferometer) has the potential for making direct observation EGPs around nearby stars, if it is limited by the fundamental noises. This method gains from previous data obtained from RV observations and will be used for getting low-resolution spectroscopy, planetary mass and inclination rather than for new discoveries.

The most favourable targets are the hot EGPs, or 'Pegasi' planets, which orbit at a short distance from their star. More than a dozen of such objects could be observed with AMBER/VLTI in the near-IR. In the mid-IR, the thermal background imposes a strong limit and only a handful, if any, of objects might be observable with MIDI/VLTI in a reasonable time. As the irradiation from the star, and thus the effective temperature of the planet, decreases fast with orbital distance, we estimate that EGPs at separation larger than 0.2 au cannot be observed by that method from the current long-baseline interferometers.

Using an appropriate observation procedure, differential interferometric measurements of EGPs are expected to be unaffected by the astrophysical biases. On the other hand, the variable chromatic effects from the instrument and the atmosphere will be significantly higher than the astrophysical signal, and therefore require to be properly calibrated and/or corrected. From our theoretical and early observational results, we estimate that the goal of getting a precision close to the fundamental noise limits can be achieved on colour-differential phase from single baselines, as soon as the current VLTI stabilization work is concluded. The standard deviation of the phase for each spectral channel is currently less than twice the photon noise over a fast-calibration period. This fundamental precision can be improved with a better control of the VLTI jitter and reduced overheads. Chromatic effects from atmospheric and instrumental origin will then dominate the error budget. If we are strictly limited by the current performances, only planets brighter than 10^{-3} times the stellar flux can be observed. However, on AMBER we expect to obtain very soon a closure phase at least as good as the current differential phases, which would lead to 18 h of observation for the currently estimated flux of 'Pegasi' planets. If the other calibration techniques that we are testing (beam commutation, fit of the atmospheric dispersion) work as expected, then this interval should be reduced to less than 2 h. We therefore consider the spectroscopy of the most favourable hot giant planets with large interferometers as a short-term perspective.

On a further perspective, a space-borne instrument for using colour-differential measurements would present an enormous improvement. It would suppress all the chromatic dispersion effects from the air and would largely increase the range of the potential targets, by giving access to the mid-IR with a low thermal noise.

ACKNOWLEDGMENTS

We are grateful to T. Barman, F. Allard and T. Guillot for their help on giant planet models. We also thank the members of the AMBER consortium for their support on the colour-differential aspects of the instrument and the ESO/VLTI team for their support during the observations.

REFERENCES

Aigrain S., Favata F., Gilmore G., 2004, A&A, 414, 1139
Akeson R. L., Swain M. R., Colavita M. M., 2000, SPIE, 4006, 321
Barman T. S., Hauschildt P. H., Allard F., 2001, ApJ, 556, 885
Beckers J. M., Hege E. K., 1982, IAU Coll. 67, Instrumentation for Astronomy with Large Optical Telescopes. Reidel Dordrecht, p. 199
Brown T., Charbonneau D., Gilliland R., Noyes R., Burrows A., 2000, ApJ, 552, 699
Charbonneau D. et al., 2005, ApJ, 626, 523
Chauvin G., Lagrange A.-M., Dumas C., Zuckerman B., Mouillet D., Song I., Beuzit J.-L., Lowrance P., 2004, A&A, 425, L29
Chelli A., Petrov R. G., 1995a, A&AS, 109, 389
Chelli A., Petrov R. G., 1995b, A&AS, 109, 401
Ciddor P. E., 1996, Ap. Opt., 35, 1566
Colavita M. M., Swain M. R., Akeson R. L., Koresko C. D., Hill R. J., 2004, PASP, 116, 876
Cumming A., 2004, MNRAS, 354, 1165
Deming D., Seager S., Richardson L. J., Harrington J., 2005, Nat, 434, 740
Derie F., Delplancke F., Glindemann A., Lévêque S., Ménardi S., Paresce F., Wilhelm R., Wirenstrand K., 2003, in Lacoste H., ed., ESA SP-522, Genie-Darwin Workshop-Hunting for Planets. ESA Publications Division, Noordwijk, p. 61
Guillot T., 1999, Sci, 286, 72
Lagarde S., 1994, PhD thesis, Univ. Nice-Sophia Antipolis
Leinert C. et al., 2003, Ap&SS, 286, 73
Lineweaver C. H., Grether D., 2003, ApJ, 598, 1350
Lopez B., Petrov R. G., 2000, in Bergeron J., Renzini A., eds, Proc. ESO Symp., From Extrasolar Planets to Cosmology. Springer-Verlag, Berlin, p. 565
Lopez B. et al., 2003, SPIE, 4838, 1011
Lund G., Aime C., 1988, Opt. Commun., 67, 79
Mayer L., Quinn T., Wadsley J., Stadel J., 2002, Sci, 298, 1756
Mayor M., Queloz D., 1995, Nat, 378, 355
Meisner J. A., Le Poole R. S., 2003, SPIE, 4838, 609
Millour F., Petrov R. G., Vannier M., 2006, in Aime C., Vakili F., eds, IAU Coll. 200, Direct Imaging of Exoplanets: Science and Techniques. Cambridge Univ. Press., Cambridge, in press
Mourard D., Bosc I., Labeyrie A., Koechlin L., Saha S., 1989, Nat, 342, 520
Petrov R. G., 1989, in Alloin D., Mariotti J. M., eds, NATO ASIC Proc. 274: Diffraction-Limited Imaging with Very Large Telescopes. Kluwer, Dordrecht, p. 249
Petrov R., Roddier F., Aime C., 1986, Opt. Soc. Am. J., 3, 634
Petrov R. G., Vannier M., Lopez B., Bresson Y., Robbe-Dubois S., Lagarde S., 2003, Aime C., Soummer R., eds, EAS Publications Ser. Vol. 8, Astronomy with High Contrast Imaging, p. 297
Petrov R. G. et al., 2003, SPIE, 4838, 924

Sánchez L. J., Petrov R. G., Vasyuk V., Lagarde S., Blazit A., Cuevas S., Foy R., 1997, Proc. ESO Workshop, Science with the VLT Interferometer. ESO, Garching, p. 393
Ségransan D., Beuzit J., Delfosse X., Forveille T., Mayor M., Perrier-Bellet C., Allard F., 2000, SPIE, 4006, 269
Showman A. P., Guillot T., 2002, A&A, 385, 166
Sorokin L. Y., Tokovinin A. A., 1985, Pis ma Astronomicheskii Zhurnal, 11, 542
Stepinski T. F., Black D. C., 2000, A&A, 356, 903
Swain M. R., Akeson R. L., Colavita M. M., Shao M., 2000, in Penny A. J., Artymowicz P., Lagrange A.-M., Russell S., eds, Proc. IAU Symp. 202, Planetary Systems in the Universe – Observation, Formation and Evolution. Astron. Soc. Pac., San Francisco, p. 103
Takami M., Bailey J., Chrysostomou A., 2003, A&A, 397, 675
Thom C., Granes P., Vakili F., 1986, A&A, 165, L13
Tubbs R. N., Meisner J. A., Bakker E. J., Albrecht S., 2004, SPIE, 5491, 588
Tubbs R., 2005, Appl. Opt., 44, 6253
Vakili F., Bonneau D., Lawson P. R., Merlin G., Mourard D., Stee P., Vallee F., Tallon-Bosc I., 1994, SPIE, 2200, 216
Vannier M., Petrov R. G., Bensammar S., Lopez B., 2003, in Aime C., Soummer R., eds, EAS Publications Ser. Vol. 8, Astronomy with High Contrast Imaging, p. 171
Vannier M., Petrov R. G., Robbe-Dubois S., Bresson Y., Lagarde S., Lopez B., 2003, SPIE, 4838, 934
Vannier M. et al., 2005a, SPIE, 5491, 577
Vannier M., Millour F., Petrov R. G., 2005b, Proc. ESO Workshop, The Power of Optical/IR Interferometry: Recent Scientific Results and 2nd Generation VLTI Instrumentation. ESO, Garching, in press

This paper has been typeset from a TEX/LATEX file prepared by the author.